Environmental Research 279 (2025) 121767

Contents lists available at ScienceDirect

Environmental Research

journal homepage: www.elsevier.com/locate/envres

Estimating global anthropogenic CO_2 emissions through satellite observations

Jia He, Bo Huang *

Department of Geography, The University of Hong Kong, Hong Kong, China

ARTICLE INFO

Keywords:
CO_2 emission
GOSAT
Spatiotemporal modelling
GTWR

ABSTRACT

Tracking human-induced CO_2 emissions accurately is fundamental for comprehending the carbon cycle and formulating effective mitigation strategies for achieving carbon neutrality. Observations from satellites present a potentially unbiased and efficient solution compared to the prevailing self-reporting approach. This study presents a novel approach for estimating anthropogenic emissions using satellite-based CO_2 measurements and the geographically and temporally weighted regression (GTWR) model. The GTWR model innovatively integrates both spatial and temporal variations to better capture the spatial heterogeneity and temporal dynamics of CO_2 emissions. Column-averaged CO_2 (XCO_2) measurements from the Greenhouse Gases Observing Satellite (GOSAT) and several environmental parameters are used as predictors in this model. Validation against the Open-source Data Inventory for Anthropogenic CO_2 (ODIAC) data shows high correlation ($R^2 = 0.929$), highlighting the significant potential of direct satellite estimations in enhancing emissions tracking. Comparisons with ODIAC, the Emission Database for Global Atmospheric Research (EDGAR), and co-emitted NO_2 from OMI/Aura reveal consistent patterns and trends, demonstrating the reliability of this approach. This consistency further corroborates the effectiveness of satellite-based estimations in quantifying anthropogenic CO_2 emissions, which is essential for monitoring carbon cycle and developing mitigation policies. The satellite-based estimations demonstrate high correlation and consistency, providing a robust foundation for objectively assessing global carbon emission mitigation policies. Future enhancements in spatial resolution and reduced dependence on existing inventories will further strengthen the reliability of these estimations.

1. Introduction

Carbon dioxide (CO_2) is a key greenhouse gas contributing to climate change and worldwide direct radiative forcing (Crippa et al., 2022; Pachauri and Mayer, 2015). It is evenly mixed with other atmospheric components and remains in the atmosphere for a prolonged period. The amount of CO_2 in the atmosphere has constantly risen due to human activities over the past few decades, especially those leading to fossil fuel emissions (Crippa et al., 2022; Friedlingstein et al., 2019, 2021). The Paris Agreement under the UN Framework Convention on Climate Change (UNFCCC) suggests that governments make promises to participate in greenhouse gas mitigation pledges to reduce carbon emissions and foster a sustainable, low-carbon economy. To evaluate the progress of the mitigation initiatives for different governments, a reliable monitoring system for anthropogenic CO_2 emissions is urgently needed.

To quantify CO_2 emissions, two primary monitoring approaches – referred to as 'bottom-up' and 'top-down', have been established over the past few decades. 'Bottom-up' approaches are the most widely used and standardized techniques for estimating CO_2 emissions. This approach typically involves combining pre-established emission factors for particular sources across various activity sectors with data from other activities like fuel use or traffic monitoring. To create high-resolution CO_2 emission maps, the bottom-up inventories are downscaled using spatial proxies such as population density (e.g. MIX, Li et al., 2017), geographical information, including the locations of point emission sources and road networks (e.g. EDGAR, Crippa et al., 2022), and nighttime lights (e.g. ODIAC, Oda et al., 2018). However, it's difficult to ensure the precision and reliability of the estimated emissions because of the varying capacity and quality of emission inventories both within and between nations (Xu, 2020).

'Top-down' approaches provide a global perspective on CO_2 emissions. This method functions by analyzing atmospheric CO_2 concentration levels collected from satellites or ground-based stations and working backwards to estimate the emission sources and quantities.

* Corresponding author.
E-mail address: bohuang@hku.hk (B. Huang).

https://doi.org/10.1016/j.envres.2025.121767
Received 31 October 2024; Received in revised form 1 April 2025; Accepted 2 May 2025
Available online 8 May 2025

Notably, observations from space-based remote sensing satellites provide additional data that complement the existing global network of ground-based greenhouse gas monitoring systems (Cogan et al., 2012; Crowell et al., 2019; Yang et al., 2021). The positive correlation between CO_2 anomalies derived from Orbiting Carbon Observatory-2 (OCO-2) and the emission data obtained from ODIAC underscores the viability of using satellite data for tracking CO_2 emissions (Hakkarainen et al., 2016). Various atmospheric models are used in conjunction with satellite data to estimate CO_2 emissions (Nassar et al., 2011; Lauvaux et al., 2016; Basu et al., 2018), but the accuracy of these models are heavily dependent on empirical data and highly sensitive to initial and boundary conditions, which significantly limit their applicability for globally characterizing carbon emissions. Statistical models offer a more abstract approach using traditional regression techniques and spatial analysis methods. For instance, CO_2 emissions are estimated with satellite-derived data from GOSAT using a general regression neural network model (Yang et al., 2019), while a multiple linear regression model is used to estimate emissions from OCO-2 XCO_2 data (Pan et al., 2021). Unfortunately, the discrepancies between the modeled data and emission inventories, along with the infrequent estimation intervals, indicating that these approaches struggled to capture the spatial heterogeneity and temporal variations within the emission data.

To address the limitations inherent in earlier models, this research introduces an innovative approach for the direct estimating global anthropogenic emissions through the integration of the GTWR model. Using multi-year XCO_2 data obtained from GOSAT, this model uniquely combines data containing temporal information with spatial variations using a spatial-temporal weighting approach. This approach offers a robust global representation of carbon emissions, significantly enhancing traditional models by capturing both local variations and temporal dynamics. The modeled results are validated against ODIAC, and detailed intercomparisons with EDGAR inventories are discussed. Furthermore, the correlation with co-emitted NO_2 is examined to further evaluate the accuracy of the emission estimates.

2. Data and methodology

2.1. Datasets

2.1.1. GOSAT XCO_2

The XCO_2 retrieved from satellite-based observations represent the total amount of CO_2 in the atmosphere. This research uses XCO_2 data retrieved from GOSAT, launched in January 2009, for the estimation process (Patra et al., 2021; Yokota et al., 2009). The thermal and near-infrared sensor for carbon observation-Fourier-transform spectrometer (TANSO-FTS) onboard the satellite quantifies CO_2 through observing surface reflectance in the short wave infrared bands in cloudless circumstances over the land area (Yokota et al., 2009). Several GOSAT XCO_2 products were developed using global atmospheric transfer model with various spatial and temporal resolutions (Kuze et al., 2016). The optimal temporal resolution to accurately capture fluctuation trends and maintain extensive global coverage was examined by analyzing the daily mean, daily median, monthly mean, and monthly median of XCO_2 observations (Fig. 1). These observations, recorded from January 2013 to December 2019 at the Caltech station, revealed significant daily fluctuations but consistent seasonal variations across all datasets. While daily data can capture immediate changes and finer-scale variations, they're more susceptible to noise and data gaps. Monthly averaging provides enhanced stability and reduces transient noise but can obscure short-term emission events. To balance the trade-offs and ensure dense and frequent sampling for the estimation process, we adopted the Level 3 monthly product of XCO_2 (FTS_C01S_3) for the following emission estimation process. The spatial resolution for this product is $2.5 \times 2.5^{\circ}$ (see Fig. 2).

2.1.2. Ancillary data

Atmospheric conditions including temperature, humidity, and atmospheric dynamics can significantly affect the dispersion and concentration of atmospheric CO_2, thus influencing the estimation of satellite-derived CO_2 emissions. Accurate estimation on CO_2 emission requires a deep understanding and thorough consideration of both these parameters and XCO_2 data. This study adopts several key atmospheric parameters namely air temperature, total column water vapor (tcwv), atmospheric dynamics (i.e. wind speed, and vertical velocity) for the following investigation (see Table 1).

Understanding the intricate interactions between the atmospheric movement and CO_2 concentrations is essential for developing effective estimates of anthropogenic emissions. Wind, for example, serves as a transport agent for CO_2, resulting in a wider distribution of emission. Previous study has suggested that high wind speeds can dilute XCO_2 signals by accelerating the dispersion of CO_2 (Zheng et al., 2020). In this study, we utilized the mean values of local wind field data at 1000, 975, and 950 hPa to represent horizontal atmospheric movement (Beirle et al., 2011; Zheng et al., 2020). Another major component is large-scale atmospheric circulation, which drives regional variations in characteristics of the gas concentration (Ma et al., 2018). Strong vertical motion promotes the dispersal of CO_2 emissions throughout the troposphere. The subsiding motion can lead to the accumulation of CO_2 near the Earth's surface by reducing vertical mixing and dispersion. Higher CO_2 concentrations can influence regional climate patterns and potentially affect biospheric CO_2 flux. Consequently, the large-scale circulation is included for our analysis, and the vertical velocity at 500 hPa (ω500) is adopted to depict this factor (Bony et al., 2004; Brogniez and Pierrehumbert, 2007). Water vapor and air temperature are also considered in the estimation process due to their significant correlation with CO_2 solubility.

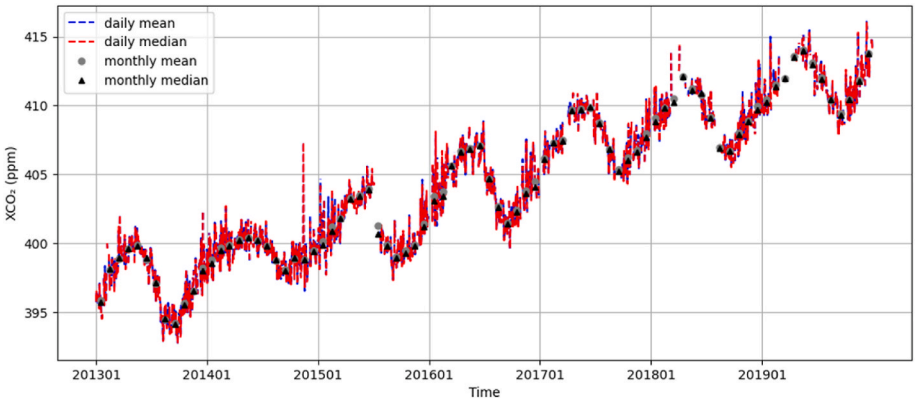

Fig. 1. Time series of the daily mean, daily median, monthly mean, and monthly median XCO_2 captured at the Caltech station from January 2013 to December 2019.

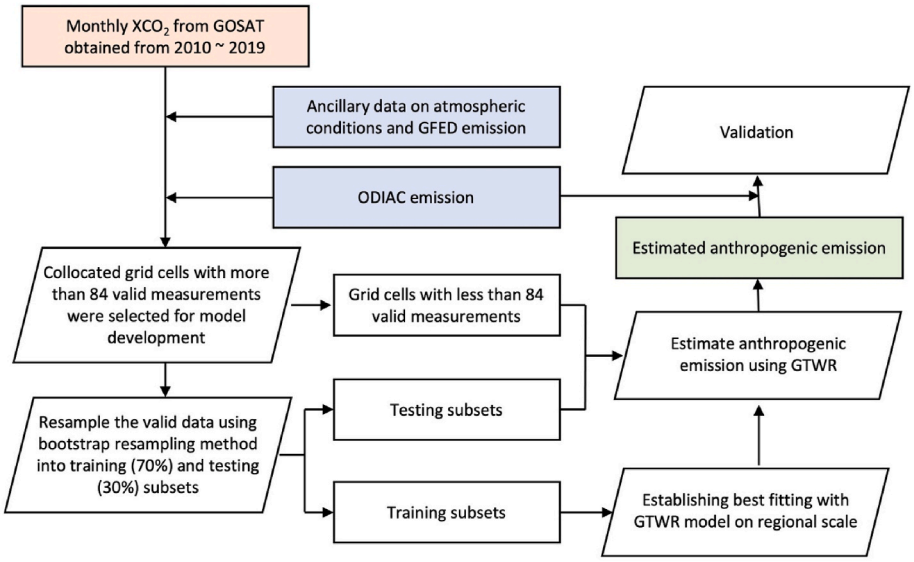

Fig. 2. Flowchart on estimation of anthropogenic emissions using satellite-based observations.

Table 1
Summary of data characteristics for parameters used in estimations on satellite-based CO_2 emissions. All data are collected with a monthly temporal resolution.

Data source	Data	Spatial Resolution	Description
GOSAT	XCO_2 (unit: ppm)	2.5 × 2.5°	Averaged CO_2 dry air mole fraction
ERA5	ω500 (unit: hPa/day)	0.25 × 0.25°	Vertical velocity at 500 hPa
	Wind speed (unit: m/s)	0.25 × 0.25°	u-component of wind at 1000, 975, and 950 hPa
	Air temperature (unit: °C)	0.5 × 0.5°	Mean monthly near-surface temperature
	Total column water vapor (unit: kg/m^2)	0.25 × 0.25°	Total column of vertically integrated water vapor
GFED	Carbon Fire emissions (unit: gC/m^2/month)	0.25 × 0.25°	Monthly emissions from biomass burning
ODIAC	Anthropogenic emissions (unit: gC/m^2/d)	1 × 1°	CO_2 emissions from fossil fuel combustion, cement production, and gas flaring
EDGAR	Anthropogenic emissions (unit: kg/m^2/s)	0.1 × 0.1°	Annual total CO_2 emissions

These data are collected from ERA5 in our study because it offers accurate global atmospheric reanalysis, providing detailed insights into the parameters (Hersbach et al., 2020). To match the resolution of the reanalysis data with the GOSAT output that we adopted in this study, the monthly averaged data was employed, even though ERA5 also contains datasets with hourly and daily estimations. Additionally, the datasets obtained from multiple resources were re-grided to 2.5 × 2.5° resolution for further estimation.

In addition to the previously mentioned parameters, the estimating technique also incorporates the Global Fire Emissions Database (GFED). This dataset is the carbon emission from fires derived based on burned-area outputs from Moderate Resolution Imaging Spectroradiometer (MODIS) (Giglio et al., 2013; Jones et al., 2020; Shi et al., 2015). Here we selected the monthly GFED data at 0.25 × 0.25° resolution for further analysis, and the dataset was re-grided to unify the spatial resolution with other datasets.

Since there is no ground truth on CO_2 emissions, the ODIAC product is used as the reference data. This product is selected because it is the only emission inventory that satisfies the criteria of Ciais et al. (2015) and is widely used for both global and regional atmospheric inversion (e.g. Thompson et al. (2016)). The ODIAC product offers a high-resolution, bottom-up inventory of global fossil fuel CO_2 emissions. This emission inventory combines individual power plant emission/location profiles with nighttime light data observed from space to estimate worldwide geographic extent of CO_2 emissions associated to fossil fuels (Oda et al., 2018). While we recognize that the ODIAC grided product may have emission modeling errors and uncertainties (Oda et al., 2018, 2019), we believe these errors and uncertainties are minor in comparison to other gridded emission inventories. It is important to note that the validation against ODIAC is calculated to identify potential issues in our estimation data records.

To further assess the consistency and the reliability of the emission estimates, intercomparisons with additional emission inventory were conducted. Emission Database for Global Atmospheric Research (EDGAR) is an emission dataset estimated using the bottom-up model incorporating a wide range of data sources, including national and international energy statistics, industrial production data, and activity data from various sectors such as agriculture, waste, and land use (Crippa et al., 2019, 2020). EDGAR CO_2 emissions dataset provides annual reports at a 0.1° × 0.1° latitude-longitude grid, offering insights into the patterns and trends of CO_2 emissions. This information is crucial for understanding the impact of human activities on climate change. To standardize all emission datasets, the intercomparison is conducted using annual emissions at 2.5° grid resolution.

2.2. Methodology

The goal of this research was to use the GTWR model on enhanced XCO_2 to directly estimate anthropogenic CO_2 emissions. The estimation process began with background removal, where the monthly median mean XCO_2 of each subregion was used as the baseline CO_2 fluxes. By subtracting these at each grid cell, the emission signals were then amplified. Key atmospheric parameters such as circulation, temperature, and humidity, along with GFED emission, were included as input parameters. To guarantee that temporal variability was adequately represented, grid cells with fewer than 84 observations were not included in the model training process. The GTWR model was utilized for the estimation from satellite data. ODIAC emissions data served as a reference for developing and validating the model. Lastly, the derived emission estimates were verified against the ODIAC emissions, which ensured the robustness and accuracy of the estimation process.

2.2.1. Parameter optimization

The measurement of anthropogenic CO_2 emissions is significantly complicated by the seasonal of variation patterns, the long atmospheric lifespan, and substantial fluctuations in the background of the atmosphere (Hakkarainen et al., 2016; Pan et al., 2021; Streets et al., 2013). To constrain the CO_2 emission from human activities, ΔXCO_2 was computed to amplify the emissions signals. It is essential to note that the estimation of CO_2 emissions not only hinges on the ΔXCO_2 data collected from satellite observations but is also intricately linked to atmospheric conditions. Examining the correlation between CO_2 emissions and the input parameters allows us to comprehend the various factors affecting CO_2 emissions and their respective effects. This, in turn, provides greater precision in model training, as well as the final emission estimates.

The compositions of ODIAC emissions data were examined by breaking down the emissions data into various intervals based on the input parameters. The analysis of the mean of CO_2 emissions within each interval showed that the evolution of CO_2 emissions was associated with the atmospheric variables. As shown in (Fig. 3a), the CO_2 emissions were positively correlated with ΔXCO_2, as the emissions increased as ΔXCO_2 rose. The conflicting results for the intervals with high ΔXCO_2 may be attributed to the restricted valid data points allocated within the intervals. Similar growth patterns in the mean value of CO_2 emissions were noted for both air temperature and tcwv, suggesting that CO_2 emissions and these two meteorological variables are positively correlated. The results of the decomposition based on the vertical velocity of ω500 revealed that areas with high level of CO_2 emissions tend to experience strong subsiding motion (ω500 $>$ 50 hPa/day). Conversely, low CO_2 emissions were linked to areas with the ascending motion in the atmosphere. Additionally, the results also indicate that the CO_2 emissions and fire emissions were negatively correlated.

While satellite observations provide unprecedented global coverage for CO_2 observations, space-based sampling is constrained by the factors such as cloud cover, low solar radiances at high latitudes, aerosol interference, and the challenges in accurately characterizing surface properties using retrieval algorithms (O'Dell et al., 2018). The first step in the data processing was to clean the data by removing the cloud-blocked data in the satellite observations. This step was followed by the collection of collocated data pairs for the observation period 2010 to 2019. A total of 118,390 sample groups were collected through this process (Fig. 4). illustrates the map of the valid data pairs in each grid cell throughout the observation period, highlighting an uneven global distributed of the dataset. Specifically, regions with frequent cloud cover, such as tropical rainforest and high latitude regions are systematically undersampled, therefore leading to an incomplete picture of CO_2 variability and trends in these regions. To address this, the GTWR model was adopted to handle the uneven distribution of the data, both spatially and temporally. GTWR is designed to account for spatial and temporal heterogeneity in the data, providing more accurate and localized estimates. Additionally, to better implement the GTWR model, the grid cells with over 84 valid measurements (accounting for more than 70 % of the observation period) were divided using the bootstrap resampling method into training (around 70 %, 46,341 samples) and testing (around 30 %, 19,860 samples) subsets. These subsets were then used to develop the estimation model and to validate the performance of the model output, whereas the remaining data were reserved exclusively for model validation. The purpose of the resampling step for the dataset was to retain enough data points that could accurately capture the spatial and temporal changes, reduce the impact of varying spatial distribution and satellite observation biases, while creating independent training and testing subsets (Batista et al., 2004). Notably, no grid cells in the high-latitude region had more than 84 measurements; thus emissions from this area were excluded from this study.

2.2.2. XCO_2 enhancement

As the fluctuation in the total CO_2 column concentration may be affected by multiple emission sources and sinks, the initial and most important step in estimating anthropogenic CO_2 emission is to eliminate the large-scale influence (referred to as the "background"), retaining only the XCO_2 signatures that are generated locally (Streets et al., 2013). A constant background XCO_2 over a period was often used when dealing with satellite data (Kort et al., 2012; Hakkarainen et al., 2016; Ye et al., 2020). To separate the anthropogenic emissions from CO_2 columns, the monthly median of the sub-region was extracted and used as the background CO_2 fluxes (see Fig. 5). Then the enhanced XCO_2 (ΔXCO_2) was calculated by subtracting the background from each grid cell (Hakkarainen et al., 2016):

$$\Delta XCO_2 = XCO_2(individual) - XCO_2(monthly\ median) \quad (1)$$

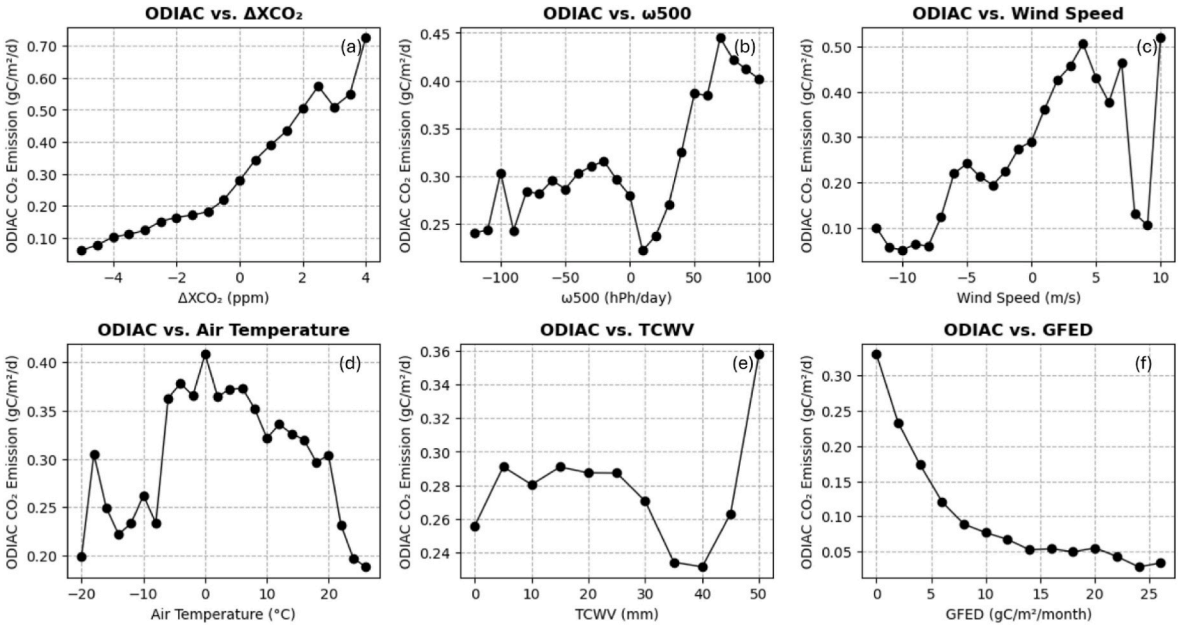

Fig. 3. Compositions of ODIAC CO_2 emissions across various intervals based on input parameters: (a) ΔXCO_2; (b) vertical velocity of ω500; (c) wind speed; (d) air temperature; (e) tcwv; (f) fire carbon emissions during 2010–2019 globally.

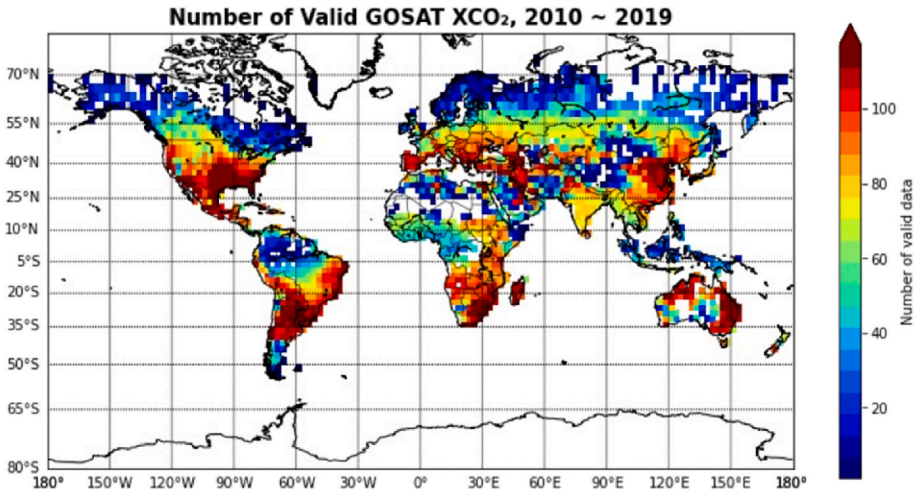

Fig. 4. Map for the valid sample groups collected during 2010–2019. The color bar represents the number of valid data.

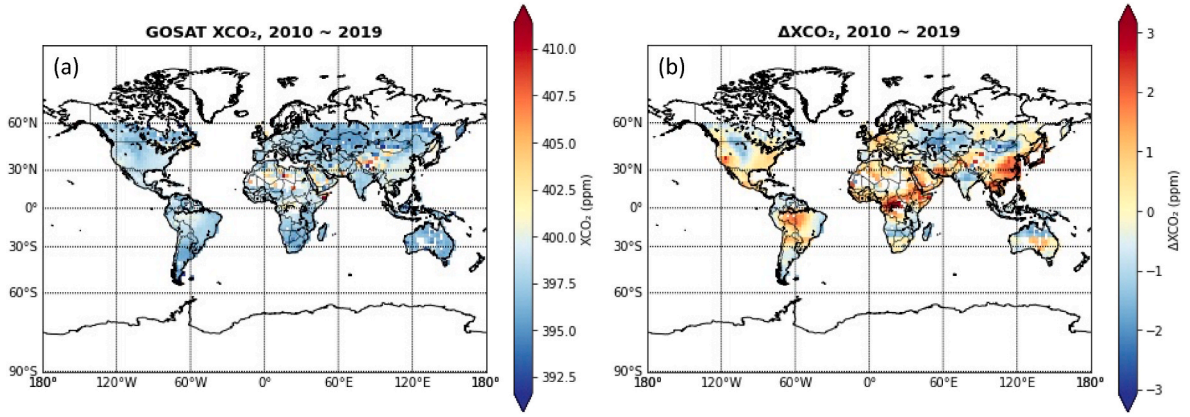

Fig. 5. Distribution map of (a) XCO_2; (b) ΔXCO_2 during 2010–2019.

This process reduces the influence of any regional scale biases in the GOSAT product while detrending the XCO_2 data. It is also important to note that based on the geographic locations and climatic characteristics, we identified seven sub-regions in this study as follows: the Tropics (between 23 °S and 23 °N), North America (from 23 °N to 60 °N, and from 180 °W to 60 °W), Mediterranean (from 23 °N to 60 °N, and from 0° to 60 °E), East Asia (from 23 °N to 60 °N, and from 60° to 180 °E), South America (from 23 °S to 60 °S, and from 90 °W to 30 °W), Africa (from 23 °S to 60 °S, and from 0° to 60 °E), and Oceania (from 23 °S to 60 °S, and from 90 °E to 180 °E).

2.2.3. GTWR model

Considering the global scale of estimation in this study, a statistical method called the GTWR is utilized to mathematically describe the relationship between satellite-derived ΔXCO_2 as well as several environmental parameters and the CO_2 emissions (He and Huang, 2018; Huang et al., 2010; Wu et al., 2021). Unlike traditional regression models that assume constant relationships (Yang et al., 2019; Pan et al., 2021), the GTWR model estimates localized parameters that can capture local variations, providing a more detailed understanding of spatio-temporal relationships. The physical basis of the GTWR model lies in the assumption that the relationships between the dependent and independent variables vary due to different local conditions, processes, and factors that influence the variables. It employs a distance-based kernel function (Gaussian) to weight observations based on both their spatial and temporal proximity to the location and period being modeled. It assigns higher weights to observations that are closer in space and time to the target location and time point. Therefore, the GTWR model can provide more accurate and detailed insights into emission estimation. Since ΔXCO_2 may result from multiple factors like the natural CO_2 fluxes, atmospheric transportations, and anthropogenic activities, the anthropogenic emissions can be expressed as:

$$\begin{aligned} AE_i = {} & \beta_0(\mu_i,\nu_i,t_i) + \beta_1(\mu_i,\nu_i,t_i) \times \Delta XCO_{2i} + \beta_2(\mu_i,\nu_i,t_i) \times \omega 500_i \\ & + \beta_3(\mu_i,\nu_i,t_i) \times WS_i + \beta_4(\mu_i,\nu_i,t_i) \times AT_i + \beta_5(\mu_i,\nu_i,t_i) \times TCWV_i \\ & + \beta_6(\mu_i,\nu_i,t_i) \times FE_i + \varepsilon_i \end{aligned} \tag{2}$$

where AE_i are the ODIAC CO_2 emissions of the sample i that located at (μ_i,ν_i) and time t_i. β_0 is the intercept of the relation at the place (μ_i,ν_i) and time t_i. β_1–β_6 denote the slopes for each input parameters at a certain place and time, respectively. The offset is represented by ε_i.

To further examine the input parameters in the model, a series of analysis were conducted with multiple combinations of input variables

Table 2
Summary of the results with different combinations of input variables in the estimation using GTWR model. The coefficient of determination (R^2) is calculated against ODIAC.

Input variables	R^2
ΔXCO_2	0.769
ΔXCO_2, WS, ω500	0.877
ΔXCO_2, WS, ω500, WV, AT	0.971
ΔXCO_2, WS, ω500, WV, AT, GFED	0.972

in the tropical area (training subset), the verification results (Table 2) prove that the model is able to accurately estimate the CO_2 emissions based on the input variables, even when the variables are varied in multiple ways.

3. Results

3.1. Validation of CO_2 emissions

To analyze the differences between the newly derived satellite-based CO_2 emission estimation and ODIAC inventory data records, the mean bias (MB) can be calculated as follows:

$$MB = \frac{1}{n}\sum_{i=1}^{n}(AE_{Estimated} - AE_{ODIAC}) \tag{3}$$

where n represents the size of the dataset, $AE_{Estimated}$ represents the satellite-based estimation, and AE_{ODIAC} represents the emission obtained from ODIAC inventory.

(Fig. 6) presents the map of the MB on CO_2 emissions between satellite-based estimations and the ODIAC inventory during 2010–2019. The spatial patterns of the satellite-based estimations closely resemble those of the ODIAC product. However, underestimations were noted in high-emission regions like the British Isles, Germany, South India, East China, and the eastern United States. Even though there are discrepancies observed between these two datasets, most of the MBs fell within 0.05 gC/m^2/d, indicating the model's robustness on a global scale.

To assess the newly estimated CO_2 emissions dataset from satellite-based measurements, the coefficient of determination (R^2) was computed as:

$$R^2 = \left(\sum_{i=1}^{n}(AE_{ODIAC} - \frac{\overline{AE_{ODIAC}})(AE_{Predicted} - \overline{AE_{Predicted}})}{\sqrt{\sum_{i=1}^{n}(AE_{ODIAC} - \overline{AE_{ODIAC}})^2 (AE_{Predicted} - \overline{AE_{Predicted}})^2}}\right)^2 \tag{4}$$

where $\overline{AE_{ODIAC}}$ and $\overline{AE_{Predicted}}$ represent the mean values of ODIAC emissions and the satellite-based estimations, respectively. (Fig. 7) illustrates the verification and validation against the ODIAC inventory. The R^2 were 0.951 and 0.929 for the training and testing subsets, respectively, demonstrating that there are strong correlations between the satellite-based estimations and the ODIAC inventory data.

The detailed validation results for the satellite-based CO_2 emission estimation in each subregion are displayed in (Fig. 8). As illustrated in the figure, the estimation shows the highest agreement in South America and Africa, where the Mediterranean region shows lower agreement. Despite the minor differences in performances, the R^2 ranges between 0.875 and 0.999. This further indicates that the CO_2 emissions estimated from the proposed new approach are robust on a global scale.

3.2. Intercomparison with EDGAR CO_2 emission

Due to the absence of direct physical measurements of CO_2 emissions, it is challenging to objectively evaluate the accuracy of the estimated results. To better understand the differences among various emission estimations, an intercomparison was conducted and discussed with additional CO_2 emission inventory from EDGAR (EDGAR version 5; Crippa et al., 2019, 2020).

Scatter plots of annual CO_2 emissions among datasets are shown in (Fig. 9). The results reveal a positive correlation among these three datasets. The satellite-based CO_2 emission estimation shows a strong alignment with the ODIAC product, with an R^2 of 0.963. However, the correlation is weaker when compared with EDGAR. The distribution map of the mean bias among annual CO_2 emissions is displayed in (Fig. 10). Underestimation (blue) in satellite-based estimation and ODIAC emission compared to EDGAR is observed in central inland region of China and northern Europe, while overestimation (red) is evident in the eastern coast of China and the southeastern United States.

Uncertainties in satellite data, including instrument errors, data processing artifacts, atmospheric interferences, and other factors, can significantly impact the accuracy of emission estimates, while ancillary parameters such as meteorological data, land use factors, and other environmental variables may introduce additional variability and potential bias into the model. It is worth mentioning that the intercomparison does not account for the estimation accuracy. Discrepancies among different emission datasets may arise from differences in data

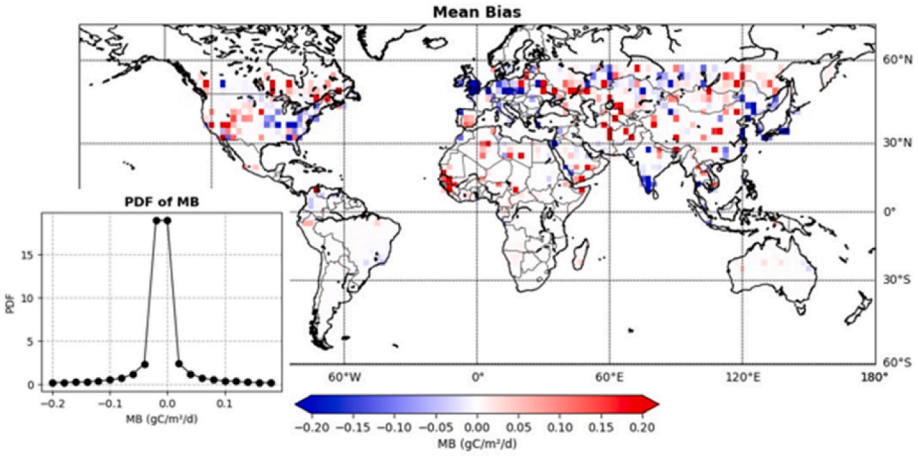

Fig. 6. Distribution map of the MB between satellite-derived emission estimations and the ODIAC emission inventory. The probability distribution function (PDF) of the MB is also presented in in the lower-right of the figure.

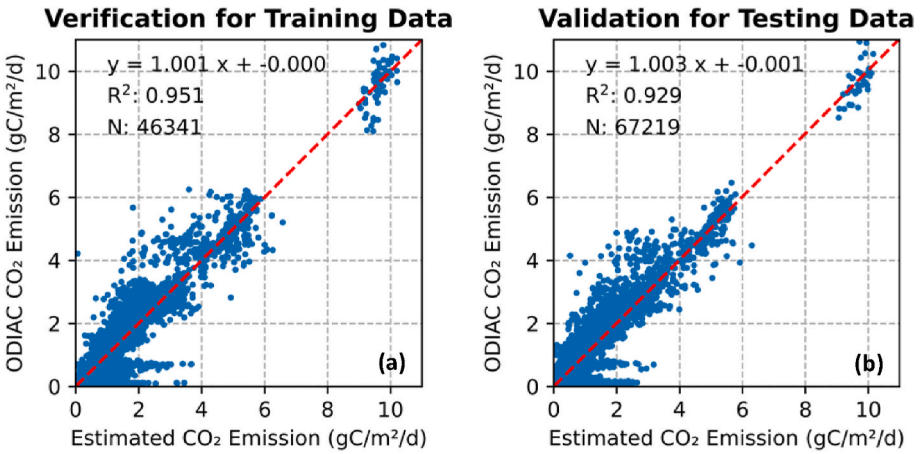

Fig. 7. Scatter plot of anthropogenic emissions for satellite-based estimation and the ODIAC inventory for (a) the training data and (b) the testing data during 2010–2019.

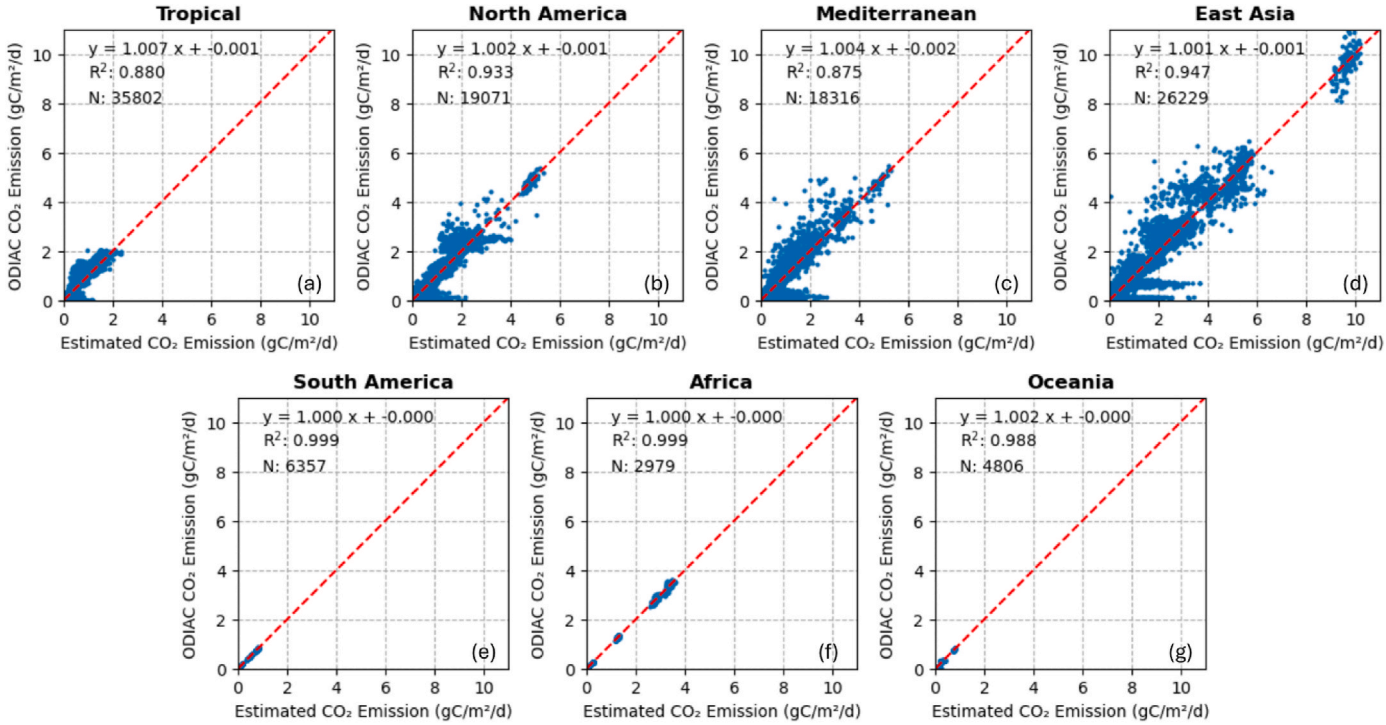

Fig. 8. Scatter plot of anthropogenic emissions for satellite-based estimations and the ODIAC inventory during 2010–2019 for each subregion (a) Tropical; (b) North America; (c) Mediterranean; (d) East Asia; (e) South America; (f) Africa; (g) Oceania.

sources, estimation methods, and the scope of emissions considered (Oda et al., 2019; Solazzo et al., 2021). Nevertheless, the observed positive correlation among EDGAR, ODIAC, and satellite-based estimation has implications for understanding global emission patterns.

3.3. Comparison with Co-emitted NO_2

It is imperative to underscore that the satellite-based estimates of CO_2 emissions are partially dependent on inventory data, as this data is used in the model training process. However, these estimates also adjust based on information collected from atmospheric observations. To fully understand the potential, benefits, and drawbacks for the proposed satellite-based CO_2 emission method, a comprehensive comparison is made with the global characteristics of other existing emission datasets, including the co-emitted NO_2 dataset. Such analysis allows for the identification of any systematic biases or errors in different estimation approaches. Additionally, the comparison can reveal areas where the satellite-based method excels or falls short.

Nitrogen dioxide (NO_2) and CO_2 emissions are interconnected, as both gases are primarily produced from the combustion of fossil fuels. Due to the short lifespan of NO_2 in the atmosphere, its vertical column densities often far exceed background levels near emission sources, making it an effective tracer for CO_2 emissions (Reuter et al., 2014, 2019). As there is no direct measurement for CO_2 emissions, comparing them with NO_2 allows for an analysis of the performance of CO_2 emission estimates. The level 3 daily measurement on global NO_2 from the Ozone Monitoring Instrument (OMI) onboard NASA's Aura satellite is employed (Lamsal et al., 2021).

A comparison was conducted to analyze the correlation between atmospheric NO_2 and CO_2 emission estimations. The normalized

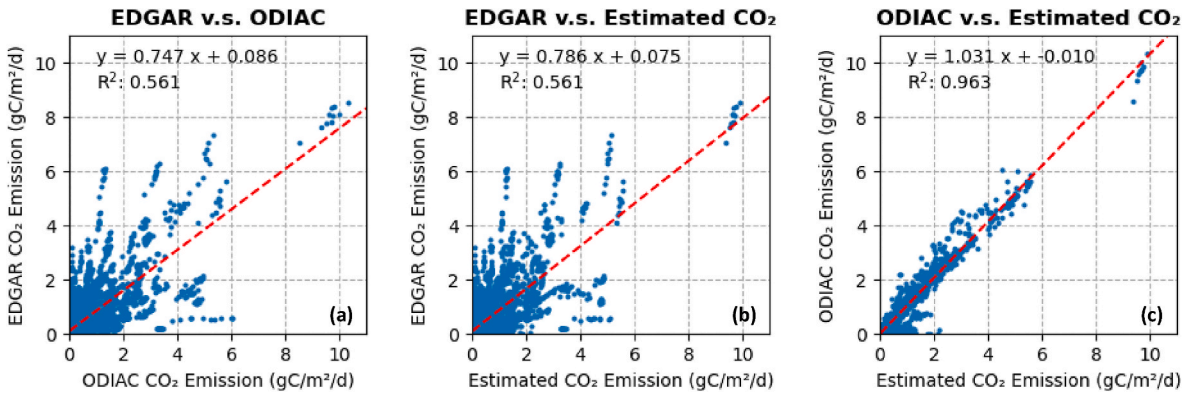

Fig. 9. Scatter plot of annual CO_2 emissions during 2010–2019 between (a) EDGAR and ODIAC; (b) EDGAR and satellite-based estimation; (c) ODIAC and satellite-based estimation.

frequencies of occurrence for the comparison are shown in (Fig. 11). The results reveal varying correlation strengths between NO_2 and the three CO_2 estimations. A moderately positive relationship was observed for NO_2 and ODIAC, with an R^2 value of 0.609. Similarly, an R^2 value of 0.632 was found for NO_2 and the satellite-based estimation. This slightly higher R^2 value can be attributed to the methodology used in the satellite-based estimation model, which employs ODIAC data as prior information for model development, thereby incorporating the same base information. Moreover, the satellite-based estimation integrates direct space-based observations to refine the results, making them more reflective of the actual atmospheric conditions, hence results in a higher correlation with NO_2 emissions. Additionally, the strongest correlation was found between NO_2 and EDGAR, with an R^2 value of 0.848. This high correlation is largely due to differences in the modeling approach between EDGAR and ODIAC. EDGAR compiles emission sectors from various data sources which are also sources of NO_2, leading to a stronger correlation.

These results demonstrate that NO_2 can serve as an effective tracer for CO_2 in regions where their emissions originated from shared sources, while also underscoring the impact of methodological variations across emission inventories. However, the applicability of using NO_2 as a universal tracer is limited, especially in areas where CO_2 and NO_2 emissions are not directly linked. Integrating NO_2 data with additional tracers and high-resolution observations can improve the reliability and precision of emission estimates.

4. Discussions

4.1. Global CO_2 emission trend

Each emission dataset, including EDGAR, ODIAC, and our satellite-based estimation, represents a unique interpretation of various inputs and assumptions, which can lead to discrepancies when compared. EDGAR utilizes a bottom-up approach, combining activity data, sector-specific emission factors, and spatial proxies (e.g. population density, road network) to provide a comprehensive global emission inventory. ODIAC, one the other hand, primarily relies on nighttime light data from satellites as spatial proxy for fossil fuel emissions, supplemented by point source data and national emission statistics. In contrast, the satellite-based estimation adopts a top-down approach, deriving emissions from atmospheric CO_2 concentrations observed by GOSAT, and the GTWR model was adopted to extract patterns and relationships from the data rather than simply replicate ODIAC emissions. This approach allows the satellite-based estimates to reflect real-world CO_2 dynamics, which are influenced by a variety of factors beyond the ODIAC dataset. These differences in methodology, data granularity, and underlying assumptions lead to variations in emission estimates.

The global CO_2 emission trends have been observed through the time series analysis of global annual mean CO_2 emissions from various sources, including ODIAC, satellite-based estimations, and EDGAR for the period of 2010–2019. As shown in (Fig. 12), the EDGAR (blue) data consistently presents higher emissions compared to the other two datasets. The reason for the disparity is that the EDGAR model includes more sectors in the estimation process. All datasets indicate an increasing trend in CO_2 emissions, yet the two bottom-up inventories, ODIAC (black) and EDGAR, exhibit a higher increasing rate compared to the satellite-based estimation. The satellite-based estimation, due to its inherent limitations, may not affectively capture diffused or less detectable emission sources from space. For instance, emissions from small-scale industrial activities, residential heating, or agricultural practices often lack the intensity or spatial concentration required for clear detection by satellites. Additionally, satellite-based methods rely on atmospheric CO_2 measurements, which can be influenced by factors such as weather patterns, atmospheric transport, and background variability, complicating the attribution of emissions to specific sources. As a result, the satellite-based estimation tends to reflect a milder increase rate compared to inventory-based approaches like ODIAC and EDGAR, which directly incorporate activity data and sector-specific emission factors.

4.2. Land cover on CO_2 emission

Earth's surface varies significantly from location to location, ranging from vegetation and water bodies to different soil types. This high heterogeneity makes it challenging to estimating CO_2 emissions, as each surface type interacts differently with the emissions (Lei et al., 2021). Therefore, analysis of CO_2 emissions must consider the variety of land cover types. The land cover type product (MCD12Q1) is used to flag the surface characteristics of the grid cells (https://doi.org/10.5067/MODIS/MCD12Q1.006). More specifically, the International Geosphere-Biosphere Programme (IGBP) legend from the dataset is used for land type classification. This dataset distinguishes 17 classes of land cover types using a decision tree algorithm that utilized the 8-day MODIS Nadir BRDF-Adjusted Reflectance. The spatial resolution for the land cover dataset is initially set at 0.05°. To best accommodate the analysis in this research, the resolution has been downsampled, with the dominant land cover type representing the surface type in the coarser resolution.

The mean of the CO_2 emissions from three different sources including ODIAC (represented in black), satellite-based estimation (in red), and EDGAR (in blue), across various land cover types are shown in (Fig. 13). For all three datasets, the urban and build-up regions have the highest CO_2 emission, and the closed shrubland regions have the lowest CO_2 emission. These results validate the rationality and validity of the estimation, as the urban and built-up regions usually have high energy consumption from buildings, industries, and heavy vehicular traffic, all

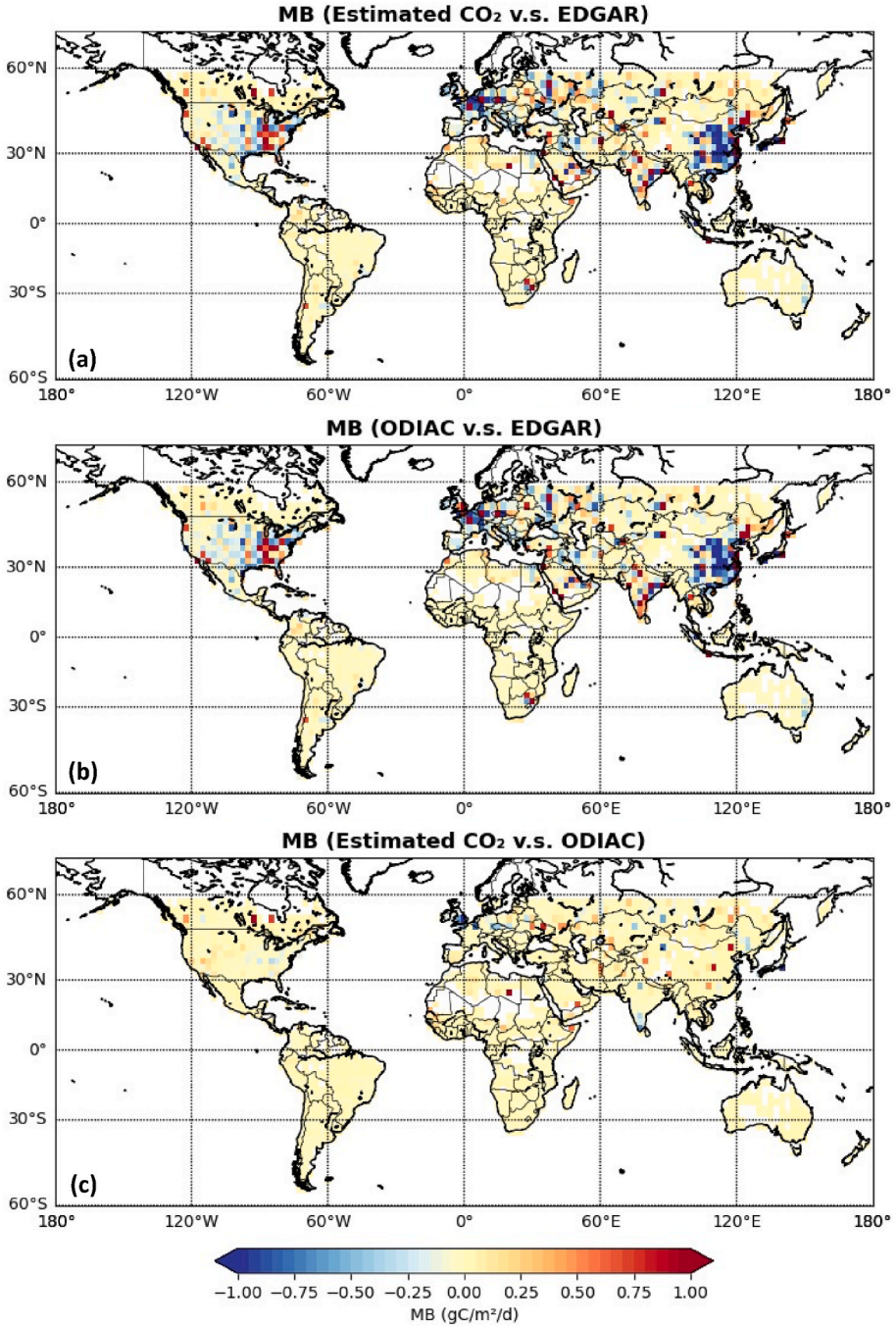

Fig. 10. Distribution map of the mean bias in annual CO_2 emissions (a) satellite-based estimation and EDGAR; (b) ODIAC and EDGAR; (c) satellite-based estimation and ODIAC.

of which typically rely on burning fossil fuels, while closed shrublands, with their vegetation and limited human activity, contribute to the lowest CO_2 emissions.

Comparisons over different land cover types are summarized (Table 3). Overall, the comparison between ODIAC and the satellite-based estimation shows better correlations, with R^2 values consistently high, indicating a close alignment. In contrast, the correlations between EDGAR and ODIAC, as well as EDGAR and the satellite-based estimation, exhibit more variability, with lower R^2 values in some regions (e.g., 0.093 for deciduous needleleaf forest and 0.276 for closed shrubland). These findings highlight the varying degrees of agreement across datasets. However, discrepancies in certain land cover types, such as shrublands and grasslands, underscore the challenges in capturing emissions uniformly across diverse environments.

4.3. Limitations

While this study demonstrates the significant potential of satellite-based estimations for estimating anthropogenic CO_2 emissions, there are several limitations must be acknowledged. Potential errors in the data sources, including satellite data and ancillary parameters, could impact the accuracy of our CO_2 emission estimation. Additionally, the coarse spatial resolution of our results can obscure small-scale emission sources, particularly in heterogeneous or complex regions. Furthermore, the reliance on emission inventories like ODIAC and EDGAR for validation introduces additional uncertainties, as these datasets may have

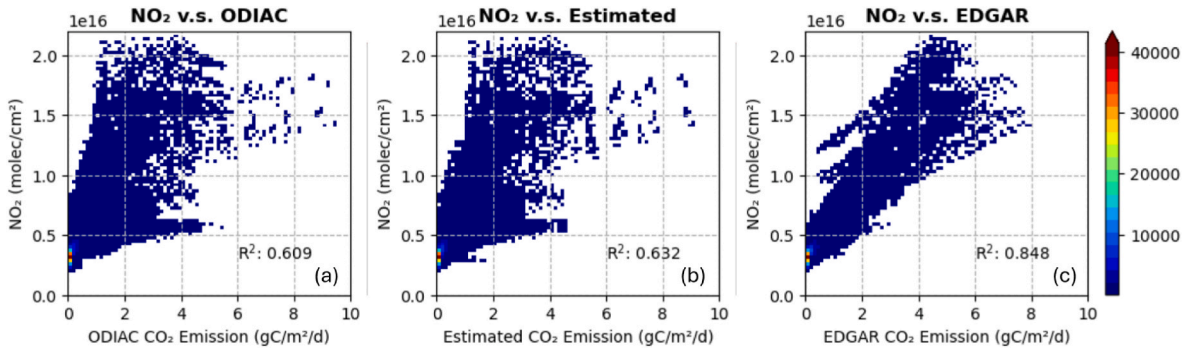

Fig. 11. Normalized frequencies of the pairs of comparison between atmospheric NO_2 from OMI/Aura and CO_2 emissions from (a) ODIAC, (b) satellite-based estimation, (3) EDGAR. The color bar represents the sample size.

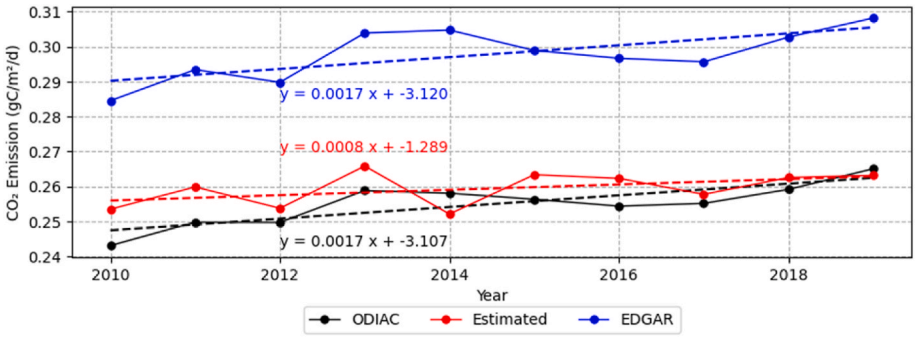

Fig. 12. Time series of global annual mean CO_2 emissions obtained from ODIAC, satellite-based estimation, and EDGAR in 2010–2019.

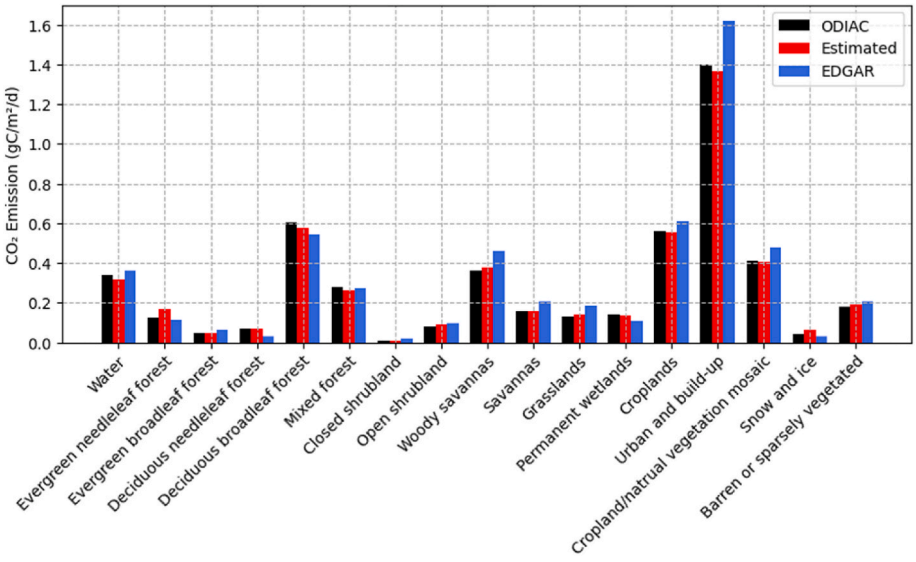

Fig. 13. The mean CO_2 emissions from ODIAC (black), satellite-based estimation (red), and EDGAR (blue) across different land cover types.

inherent biases or methodological limitations. Addressing these challenges through improved data quality, higher-resolution observations, and rigorous validating processes is essential to enhance the reliability of satellite-based emission estimations and their applicability in carbon monitoring and mitigation efforts.

5. Conclusions

Anthropogenic CO_2 emissions are directly using enhanced XCO_2 data derived from GOSAT along with atmospheric parameters as input variables using GTWR model. This data-driven strategy provides an innovative approach that uses a spatiotemporal weighting mechanism to account for both temporal and geographical variations. While this approach partially dependent on ODIAC data due to the lack of physical measurements of CO_2 emissions, offers an independent measure of carbon emissions and provides additional insights from satellite measurements, leading to more comprehensive picture of emission patterns. Also, the bootstrap resampling method is adopted to reduce any impacts from the biases in data retrieval algorithm, data point variability, and spatial dispersion. The high correlation between the estimated results

Table 3
Summary of the comparison results over different land cover types.

	EDGAR v.s. ODIAC			EDGAR v.s. Estimated CO_2			ODIAC v.s. Estimated CO_2		
	Slope	Intercept	R^2	Slope	Intercept	R^2	Slope	Intercept	R^2
Water (4907)	0.754	0.105	0.715	0.807	0.102	0.703	1.068	−0.003	0.979
Evergreen needleleaf forest (3731)	0.780	0.015	0.755	0.618	0.010	0.434	0.825	−0.013	0.624
Evergreen broadleaf forest (13,992)	1.438	−0.001	0.777	1.422	−0.007	0.750	0.992	−0.004	0.972
Deciduous needleleaf forest (160)	0.115	0.024	0.093	−0.056	0.035	0.020	0.871	0.008	0.683
Deciduous broadleaf forest (7397)	0.628	0.163	0.541	0.691	0.144	0.585	1.045	0.001	0.977
Mixed forest (11,365)	0.767	0.060	0.692	0.828	0.053	0.700	1.060	−0.003	0.974
Closed shrubland (326)	1.189	0.010	0.276	1.181	0.009	0.273	0.984	−0.001	0.973
Open shrubland (13,850)	0.543	0.051	0.469	0.496	0.049	0.457	0.883	−0.001	0.911
Woody savannas (20,639)	1.029	0.087	0.808	1.046	0.065	0.806	1.010	−0.019	0.986
Savannas (30,042)	1.061	0.041	0.769	1.109	0.032	0.770	1.035	−0.007	0.984
Grasslands (74,324)	0.852	0.075	0.456	0.854	0.063	0.449	0.975	−0.010	0.933
Permanent wetland (136)	0.549	0.030	0.959	0.559	0.030	0.945	1.016	0.002	0.980
Croplands (43,522)	0.885	0.112	0.595	0.943	0.086	0.622	1.030	−0.009	0.977
Urban and build-up (308)	0.725	0.606	0.776	0.726	0.627	0.775	1.001	0.030	0.996
Cropland/natural vegetation mosaic (2052)	0.866	0.120	0.665	0.901	0.114	0.671	1.028	−0.002	0.983
Snow and ice (64)	0.164	0.025	0.911	0.162	0.022	0.807	0.925	−0.016	0.773
Barren or sparsely vegetated (15,410)	0.668	0.089	0.468	0.713	0.074	0.441	1.049	−0.019	0.910

and ODIAC data (with an R^2 of 0.929) shows that the proposed methodology is a robust and efficient strategy for monitoring global CO_2 emissions.

To further examine the consistency, variability, and reliability of the satellite-based estimation, EDGAR, an additional emission inventory, is included for a comprehensive intercomparison. A lower estimation in the satellite-based estimation and OIDAC emission relative to EDGAR is observed in the central inland region of China and northern Europe. Conversely, an overestimation is seen along the eastern coast of China and southeastern regions of the United States. These discrepancies may result from various factors such as data reporting inconsistencies, satellite retrieval biases, or diffing calculation methodologies. The land use is another factor to discuss when comparing these three emission datasets. Urban and build-up areas have the highest CO_2 emissions due to intense energy consumption from buildings, industries, and traffic. While the closed-shrublands have the lowest emissions due to the limited human activity in these regions.

Furthermore, as there are no direct measurements for CO_2 emissions to validate the estimation accuracy, comparing them with NO_2 allows for an additional insight into the performance of CO_2 emission estimates. Moderate positive correlations are found between NO_2 and ODIAC ($R^2 = 0.609$), and NO_2 and the satellite-based estimation ($R^2 = 0.632$). A higher correlation is observed between NO_2 and EDGAR ($R^2 = 0.848$), likely due to EDGAR's approach in compiling more emission sectors than ODIAC, particularly the traffic, which is also a significant source of NO_2. These findings corroborate the reasonableness and accuracy of the emission estimations.

In conclusion, our study demonstrated a feasible approach to precisely estimate CO_2 emissions using CO_2 column quantities obtained from satellite observations. The findings carry substantial implications for applications utilizing satellite observations on CO_2 to monitor anthropogenic CO_2 emissions at various scales. Even while characterizing the real-world atmospheric dynamics based solely on the input variables of this study may appear oversimplified, the atmospheric parameters included provide a meaningful representation of atmospheric conditions, thereby making our approach easily adaptable to a worldwide setting. Future availability of satellite data with finer spatial and temporal resolutions holds great promise for enhancing our understanding and monitoring of global CO_2 emissions, ultimately contributing to environmental and climate studies.

It is worth mentioning that despite the minimal impact on anthropogenic emissions, high-latitude regions are critical to global climate systems, making enhanced data collection and analysis through methods like data fusion a key focus for future research. To further advance this field, research should leverage high-resolution satellite data to improve the precision of CO_2 emission estimates and enhance the detection of localized sources. Advances in machine learning and artificial intelligence modelling algorithms will help address uncertainties and better capture complex atmospheric dynamics, refining the accuracy of emission estimates. Additionally, integrating satellite observations with ground-based sensors and aerial platforms will provide a more comprehensive monitoring framework, significantly advancing emission monitoring and informing effective climate policies.

CRediT authorship contribution statement

Jia He: Writing – original draft, Visualization, Validation, Methodology, Investigation, Formal analysis, Data curation. **Bo Huang:** Writing – review & editing, Supervision, Resources, Project administration, Methodology, Funding acquisition, Conceptualization.

Declaration of competing interest

The authors declare that they have no known competing financial interests or personal relationships that could have appeared to influence the work reported in this paper.

Acknowledgements

This work was supported by the Research Grants Council of Hong Kong under Grant Nos. SRFS2324-4H02, GRF 14616323, GRF 17617024, TRS T22-606/23-R, and T22-607-24-N, the National Key Research and Development Program of China under Grant No. 2022YFB3903700, and the National Natural Science Foundation of China under Grant No. 42271439. The XCO_2 data were obtained from the GOSAT Project (ftp://gosat-ds.eo.esa.int/) operated by the National Institute for Environmental Studies (NIES). The ancillary data on atmospheric conditions were obtained from the European Centre for Medium-Range Weather Forecasts (ECMWF) ERA5 reanalysis products (https://cds.climate.copernicus.eu). The fire emissions data were obtained from the global fire emissions database (https://www.geo.vu.nl/~gwerf/GFED/GFED4/). The ODIAC CO_2 emissions data (https://db.cger.nies.go.jp/dataset/ODIAC/DL_odiac2020b.html) were provided by the Center for Global Environmental Research at NIES. EDGAR emissions were collected from the European Commission, Joint Research Centre (JRC)/Netherlands Environmental Assessment Agency (PBL) (https://edgar.jrc.ec.europa.eu/dataset_ghg80). The NO_2 data are collected from NASA Goddard Space Flight Center, Goddard Earth Sciences Data and Information Services Center (GES DISC) (https://disc.gsfc.nasa.gov/datasets/OMNO2d_003/summary).

Data availability

Data will be made available on request.

References

Basu, S., Baker, D.F., Chevallier, F., Patra, P.K., Liu, J., Miller, J.B., 2018. The impact of transport model differences on CO_2 surface flux estimates from OCO-2 retrievals of column average CO_2. Atmos. Chem. Phys. 18, 7189–7215. https://doi.org/10.5194/acp-18-7189-2018.

Batista, G.E.A.P.A., Prati, R.C., Monard, M.C., 2004. A study of the behavior of several methods for balancing machine learning training data. SIGKDD Explor Newsl 6, 20–29. https://doi.org/10.1145/1007730.1007735.

Beirle, S., Boersma, K.F., Platt, U., Lawrence, M.G., Wagner, T., 2011. Megacity emissions and lifetimes of nitrogen oxides probed from space. Science 333, 1737–1739. https://doi.org/10.1126/science.1207824.

Bony, S., Dufresne, J.-L., Le Treut, H., Morcrette, J.-J., Senior, C., 2004. On dynamic and thermodynamic components of cloud changes. Clim. Dyn. 22, 71–86. https://doi.org/10.1007/s00382-003-0369-6.

Brogniez, H., Pierrehumbert, R.T., 2007. Intercomparison of tropical tropospheric humidity in GCMs with AMSU-B water vapor data. Geophys. Res. Lett. 34. https://doi.org/10.1029/2006GL029118.

Ciais, P., Crisp, D., van der Gon, H., Engelen, R., Janssens-Maenhout, G., Heimann, M., Rayner, P., Scholze, M., 2015. Towards a European Operational Observing System to Monitor Fossil: CO2 Emissions. Publications Office of the European Union, LU.

Cogan, A.J., Boesch, H., Parker, R.J., Feng, L., Palmer, P.I., Blavier, J.-F.L., Deutscher, N. M., Macatangay, R., Notholt, J., Roehl, C., Warneke, T., Wunch, D., 2012. Atmospheric carbon dioxide retrieved from the greenhouse gases observing SATellite (GOSAT): Comparison with ground-based TCCON observations and GEOS-chem model calculations. J. Geophys. Res. Atmospheres 117. https://doi.org/10.1029/2012JD018087.

Crippa, M., Oreggioni, G., Guizzardi, D., Muntean, M., Schaaf, E., Lo Vullo, E., Solazzo, E., Monforti-Ferrario, F., Olivier, J.G.J., Vignati, E., 2019. Fossil CO2 and GHG Emissions of all World Countries: 2019 Report. Publications Office of the European Union, LU.

Crippa, M., Solazzo, E., Huang, G., Guizzardi, D., Koffi, E., Muntean, M., Schieberle, C., Friedrich, R., Janssens-Maenhout, G., 2020. High resolution temporal profiles in the emissions database for global atmospheric research. Sci. Data 7, 121. https://doi.org/10.1038/s41597-020-0462-2.

Crippa, M., Guizzardi, D., Banja, M., Solazzo, E., Muntean, M., Schaaf, E., Pagani, F., Monforti-Ferrario, F., Olivier, J.G.J., Quadrelli, R., Risquez Martin, A., Taghavi-Moharamli, P., Grassi, G., Rossi, S., Oom, D., Branco, A., San-Miguel, J., Vignati, E., 2022. CO2 Emissions of all World Countries: JRC/IEA/PBL 2022 Report. Publications Office of the European Union, LU.

Crowell, S., Baker, D., Schuh, A., Basu, S., Jacobson, A.R., Chevallier, F., Liu, J., Deng, F., Feng, L., McKain, K., Chatterjee, A., Miller, J.B., Stephens, B.B., Eldering, A., Crisp, D., Schimel, D., Nassar, R., O'Dell, C.W., Oda, T., Sweeney, C., Palmer, P.I., Jones, D.B.A., 2019. The 2015–2016 carbon cycle as seen from OCO-2 and the global in situ network. Atmos. Chem. Phys. 19, 9797–9831. https://doi.org/10.5194/acp-19-9797-2019.

Friedlingstein, P., Jones, M.W., O'Sullivan, M., Andrew, R.M., Hauck, J., Peters, G.P., Peters, W., Pongratz, J., Sitch, S., Le Quéré, C., Bakker, D.C.E., Canadell, J.G., Ciais, P., Jackson, R.B., Anthoni, P., Barbero, L., Bastos, A., Bastrikov, V., Becker, M., Bopp, L., Buitenhuis, E., Chandra, N., Chevallier, F., Chini, L.P., Currie, K.I., Feely, R. A., Gehlen, M., Gilfillan, D., Gkritzalis, T., Goll, D.S., Gruber, N., Gutekunst, S., Harris, I., Haverd, V., Houghton, R.A., Hurtt, G., Ilyina, T., Jain, A.K., Joetzjer, E., Kaplan, J.O., Kato, E., Klein Goldewijk, K., Korsbakken, J.I., Landschützer, P., Lauvset, S.K., Lefèvre, N., Lenton, A., Lienert, S., Lombardozzi, D., Marland, G., McGuire, P.C., Melton, J.R., Metzl, N., Munro, D.R., Nabel, J.E.M.S., Nakaoka, S.-I., Neill, C., Omar, A.M., Ono, T., Peregon, A., Pierrot, D., Poulter, B., Rehder, G., Resplandy, L., Robertson, E., Rödenbeck, C., Séférian, R., Schwinger, J., Smith, N., Tans, P.P., Tian, H., Tilbrook, B., Tubiello, F.N., van der Werf, G.R., Wiltshire, A.J., Zaehle, S., 2019. Global carbon budget 2019. Earth Syst. Sci. Data 11, 1783–1838. https://doi.org/10.5194/essd-11-1783-2019.

Friedlingstein, P., Jones, M.W., O'Sullivan, M., Andrew, R.M., Bakker, D.C.E., Hauck, J., Le Quéré, C., Peters, G.P., Peters, W., Pongratz, J., Sitch, S., Canadell, J.G., Ciais, P., Jackson, R.B., Alin, S.R., Anthoni, P., Bates, N.R., Becker, M., Bellouin, N., Bopp, L., Chau, T.T.T., Chevallier, F., Chini, L.P., Cronin, M., Currie, K.I., Decharme, B., Djeutchouang, L., Dou, X., Evans, W., Feely, R.A., Feng, L., Gasser, T., Gilfillan, D., Gkritzalis, T., Grassi, G., Gregor, L., Gruber, N., Gürses, Ö., Harris, I., Houghton, R. A., Hurtt, G.C., Iida, Y., Ilyina, T., Luijkx, I.T., Jain, A.K., Jones, S.D., Kato, E., Kennedy, D., Klein Goldewijk, K., Knauer, J., Korsbakken, J.I., Körtzinger, A., Landschützer, P., Lauvset, S.K., Lefèvre, N., Lienert, S., Liu, J., Marland, G., McGuire, P.C., Melton, J.R., Munro, D.R., Nabel, J.E.M.S., Nakaoka, S.-I., Niwa, Y., Ono, T., Pierrot, D., Poulter, B., Rehder, G., Resplandy, L., Robertson, E., Rödenbeck, C., Rosan, T.M., Schwinger, J., Schwingshackl, C., Séférian, R., Sutton, A.J., Sweeney, C., Tanhua, T., Tans, P.P., Tian, H., Tilbrook, B., Tubiello, F., van der Werf, G., Vuichard, N., Wada, C., Wanninkhof, R., Watson, A., Willis, D., Wiltshire, A.J., Yuan, W., Yue, C., Yue, X., Zaehle, S., Zeng, J., 2021. Global carbon budget 2021. Earth Syst. Sci. Data Discuss. 1–191. https://doi.org/10.5194/essd-2021-386.

Giglio, L., Randerson, J.T., van der Werf, G.R., 2013. Analysis of daily, monthly, and annual burned area using the fourth-generation global fire emissions database (GFED4). J. Geophys. Res. Biogeosciences 118, 317–328. https://doi.org/10.1002/jgrg.20042.

Hakkarainen, J., Ialongo, I., Tamminen, J., 2016. Direct space-based observations of anthropogenic CO2 emission areas from OCO-2. Geophys. Res. Lett. 43, 11400–411406. https://doi.org/10.1002/2016GL070885.

He, Q., Huang, B., 2018. Satellite-based high-resolution PM2.5 estimation over the beijing-tianjin-hebei region of China using an improved geographically and temporally weighted regression model. Environ. Pollut. 236, 1027–1037. https://doi.org/10.1016/j.envpol.2018.01.053.

Hersbach, H., Bell, B., Berrisford, P., Hirahara, S., Horányi, A., Muñoz-Sabater, J., Nicolas, J., Peubey, C., Radu, R., Schepers, D., Simmons, A., Soci, C., Abdalla, S., Abellan, X., Balsamo, G., Bechtold, P., Biavati, G., Bidlot, J., Bonavita, M., Chiara, G. D., Dahlgren, P., Dee, D., Diamantakis, M., Dragani, R., Flemming, J., Forbes, R., Fuentes, M., Geer, A., Haimberger, L., Healy, S., Hogan, R.J., Hólm, E., Janisková, M., Keeley, S., Laloyaux, P., Lopez, P., Lupu, C., Radnoti, G., Rosnay, P. de, Rozum, I., Vamborg, F., Villaume, S., Thépaut, J.-N., 2020. The ERA5 global reanalysis. Q. J. R. Meteorol. Soc. 146, 1999–2049. https://doi.org/10.1002/qj.3803.

Huang, B., Wu, B., Barry, M., 2010. Geographically and temporally weighted regression for modeling spatio-temporal variation in house prices. Int. J. Geogr. Inf. Sci. 24, 383–401. https://doi.org/10.1080/13658810802672469.

Jones, M.O., Running, S.W., Kimball, J.S., Robinson, N.P., Allred, B.W., 2020. Terrestrial primary productivity indicators for inclusion in the national climate indicators system. Clim. Change 163, 1855–1868. https://doi.org/10.1007/s10584-018-2155-9.

Kort, E.A., Frankenberg, C., Miller, C.E., Oda, T., 2012. Space-based observations of megacity carbon dioxide. Geophys. Res. Lett. 39. https://doi.org/10.1029/2012GL052738.

Kuze, A., Suto, H., Shiomi, K., Kawakami, S., Tanaka, M., Ueda, Y., Deguchi, A., Yoshida, J., Yamamoto, Y., Kataoka, F., Taylor, T.E., Buijs, H.L., 2016. Update on GOSAT TANSO-FTS performance, operations, and data products after more than 6 years in space. Atmos. Meas. Tech. 9, 2445–2461. https://doi.org/10.5194/amt-9-2445-2016.

Lamsal, L.N., Krotkov, N.A., Vasilkov, A., Marchenko, S., Qin, W., Yang, E.-S., Fasnacht, Z., Joiner, J., Choi, S., Haffner, D., Swartz, W.H., Fisher, B., Bucsela, E., 2021. Ozone monitoring instrument (OMI) Aura nitrogen dioxide standard product version 4.0 with improved surface and cloud treatments. Atmos. Meas. Tech. 14, 455–479. https://doi.org/10.5194/amt-14-455-2021.

Lauvaux, T., Miles, N.L., Deng, A., Richardson, S.J., Cambaliza, M.O., Davis, K.J., Gaudet, B., Gurney, K.R., Huang, J., O'Keefe, D., Song, Y., Karion, A., Oda, T., Patarasuk, R., Razlivanov, I., Sarmiento, D., Shepson, P., Sweeney, C., Turnbull, J., Wu, K., 2016. High-resolution atmospheric inversion of urban CO2 emissions during the dormant season of the Indianapolis flux experiment (INFLUX). J. Geophys. Res. Atmospheres 121, 5213–5236. https://doi.org/10.1002/2015JD024473.

Lei, R., Feng, S., Danjou, A., Broquet, G., Wu, D., Lin, J.C., O'Dell, C.W., Lauvaux, T., 2021. Fossil fuel CO2 emissions over metropolitan areas from space: a multi-model analysis of OCO-2 data over lahore, Pakistan. Remote Sens. Environ. 264, 112625. https://doi.org/10.1016/j.rse.2021.112625.

Li, M., Zhang, Q., Kurokawa, J., Woo, J.-H., He, K., Lu, Z., Ohara, T., Song, Y., Streets, D. G., Carmichael, G.R., Cheng, Y., Hong, C., Huo, H., Jiang, X., Kang, S., Liu, F., Su, H., Zheng, B., 2017. MIX: a mosaic Asian anthropogenic emission inventory under the international collaboration framework of the MICS-Asia and HTAP. Atmos. Chem. Phys. 17, 935–963. https://doi.org/10.5194/acp-17-935-2017.

Ma, J., Chadwick, R., Seo, K.-H., Dong, C., Huang, G., Foltz, G.R., Jiang, J.H., 2018. Responses of the tropical atmospheric circulation to climate change and connection to the hydrological cycle. Annu. Rev. Earth Planet Sci. 46, 549–580. https://doi.org/10.1146/annurev-earth-082517-010102.

Nassar, R., Jones, D.B.A., Kulawik, S.S., Worden, J.R., Bowman, K.W., Andres, R.J., Suntharalingam, P., Chen, J.M., Brenninkmeijer, C.a.M., Schuck, T.J., Conway, T.J., Worthy, D.E., 2011. Inverse modeling of CO_2 sources and sinks using satellite observations of CO_2 from TES and surface flask measurements. Atmos. Chem. Phys. 11, 6029–6047. https://doi.org/10.5194/acp-11-6029-2011.

Oda, T., Maksyutov, S., Andres, R.J., 2018. The open-source data inventory for anthropogenic CO_2, version 2016 (ODIAC2016): a global monthly fossil fuel CO_2 gridded emissions data product for tracer transport simulations and surface flux inversions. Earth Syst. Sci. Data 10, 87–107. https://doi.org/10.5194/essd-10-87-2018.

Oda, T., Bun, R., Kinakh, V., Topylko, P., Halushchak, M., Marland, G., Lauvaux, T., Jonas, M., Maksyutov, S., Nahorski, Z., Lesiv, M., Danylo, O., Horabik-Pyzel, J., 2019. Errors and uncertainties in a gridded carbon dioxide emissions inventory. Mitig. Adapt. Strategies Glob. Change 24, 1007–1050. https://doi.org/10.1007/s11027-019-09877-2.

O'Dell, C.W., Eldering, A., Wennberg, P.O., Crisp, D., Gunson, M.R., Fisher, B., Frankenberg, C., Kiel, M., Lindqvist, H., Mandrake, L., Merrelli, A., Natraj, V., Nelson, R.R., Osterman, G.B., Payne, V.H., Taylor, T.E., Wunch, D., Drouin, B.J., Oyafuso, F., Chang, A., McDuffie, J., Smyth, M., Baker, D.F., Basu, S., Chevallier, F., Crowell, S.M.R., Feng, L., Palmer, P.I., Dubey, M., García, O.E., Griffith, D.W.T., Hase, F., Iraci, L.T., Kivi, R., Morino, I., Notholt, J., Ohyama, H., Petri, C., Roehl, C. M., Sha, M.K., Strong, K., Sussmann, R., Te, Y., Uchino, O., Velazco, V.A., 2018. Improved retrievals of carbon dioxide from orbiting carbon Observatory-2 with the version 8 ACOS algorithm. Atmos. Meas. Tech. 11, 6539–6576. https://doi.org/10.5194/amt-11-6539-2018.

Pachauri, R.K., Mayer, L., 2015. Intergovernmental panel on climate change. Climate Change 2014: Synthesis Report. Intergovernmental Panel on Climate Change, Geneva, Switzerland, p. 151.

Pan, G., Xu, Y., Huang, B., 2021. Evaluating national and subnational CO2 mitigation goals in China's thirteenth five-year plan from satellite observations. Environ. Int. 156, 106771. https://doi.org/10.1016/j.envint.2021.106771.

Patra, P.K., Hajima, T., Saito, R., Chandra, N., Yoshida, Y., Ichii, K., Kawamiya, M., Kondo, M., Ito, A., Crisp, D., 2021. Evaluation of Earth system model and atmospheric inversion using total column CO2 observations from GOSAT and OCO-2. Prog. Earth Planet. Sci. 8, 25. https://doi.org/10.1186/s40645-021-00420-z.

Reuter, M., Buchwitz, M., Hilboll, A., Richter, A., Schneising, O., Hilker, M., Heymann, J., Bovensmann, H., Burrows, J.P., 2014. Decreasing emissions of NOx relative to CO2 in East Asia inferred from satellite observations. Nat. Geosci. 7, 792–795. https://doi.org/10.1038/ngeo2257.

Reuter, M., Buchwitz, M., Schneising, O., Krautwurst, S., O'Dell, C.W., Richter, A., Bovensmann, H., Burrows, J.P., 2019. Towards monitoring localized CO_2 emissions from space: co-located regional CO_2 and NO_2 enhancements observed by the OCO-2 and S5P satellites. Atmos. Chem. Phys. 19, 9371–9383. https://doi.org/10.5194/acp-19-9371-2019.

Shi, Y., Matsunaga, T., Saito, M., Yamaguchi, Y., Chen, X., 2015. Comparison of global inventories of CO2 emissions from biomass burning during 2002–2011 derived from multiple satellite products. Environ. Pollut. 206, 479–487. https://doi.org/10.1016/j.envpol.2015.08.009.

Solazzo, E., Crippa, M., Guizzardi, D., Muntean, M., Choulga, M., Janssens-Maenhout, G., 2021. Uncertainties in the emissions database for global atmospheric research (EDGAR) emission inventory of greenhouse gases. Atmos. Chem. Phys. 21, 5655–5683. https://doi.org/10.5194/acp-21-5655-2021.

Streets, D.G., Canty, T., Carmichael, G.R., de Foy, B., Dickerson, R.R., Duncan, B.N., Edwards, D.P., Haynes, J.A., Henze, D.K., Houyoux, M.R., Jacob, D.J., Krotkov, N.A., Lamsal, L.N., Liu, Y., Lu, Z., Martin, R.V., Pfister, G.G., Pinder, R.W., Salawitch, R.J., Wecht, K.J., 2013. Emissions estimation from satellite retrievals: a review of current capability. Atmos. Environ. 77, 1011–1042. https://doi.org/10.1016/j.atmosenv.2013.05.051.

Thompson, R.L., Patra, P.K., Chevallier, F., Maksyutov, S., Law, R.M., Ziehn, T., van der Laan-Luijkx, I.T., Peters, W., Ganshin, A., Zhuravlev, R., Maki, T., Nakamura, T., Shirai, T., Ishizawa, M., Saeki, T., Machida, T., Poulter, B., Canadell, J.G., Ciais, P., 2016. Top-down assessment of the Asian carbon budget since the mid 1990s. Nat. Commun. 7, 10724. https://doi.org/10.1038/ncomms10724.

Wu, S., Huang, B., Wang, J., He, L., Wang, Z., Yan, Z., Lao, X., Zhang, F., Liu, R., Du, Z., 2021. Spatiotemporal mapping and assessment of daily ground NO2 concentrations in China using high-resolution TROPOMI retrievals. Environ. Pollut. 273, 116456. https://doi.org/10.1016/j.envpol.2021.116456.

Xu, Y., 2020. Environmental Policy and Air Pollution in China: Governance and Strategy, first ed. Routledge. https://doi.org/10.4324/9780429452154.

Yang, D., Liu, Y., Feng, L., Wang, J., Yao, L., Cai, Z., Zhu, S., Lu, N., Lyu, D., 2021. The first global carbon dioxide flux map derived from TanSat measurements. Adv. Atmos. Sci. 38, 1433–1443. https://doi.org/10.1007/s00376-021-1179-7.

Yang, S., Lei, L., Zeng, Z., He, Z., Zhong, H., 2019. An assessment of anthropogenic CO2 emissions by satellite-based observations in China. Sensors 19, 1118. https://doi.org/10.3390/s19051118.

Ye, X., Lauvaux, T., Kort, E.A., Oda, T., Feng, S., Lin, J.C., Yang, E.G., Wu, D., 2020. Constraining fossil fuel CO2 emissions from urban area using OCO-2 observations of total column CO2. J. Geophys. Res. Atmospheres 125, e2019JD030528. https://doi.org/10.1029/2019JD030528.

Yokota, T., Yoshida, Y., Eguchi, N., Ota, Y., Tanaka, T., Watanabe, H., Maksyutov, S., 2009. Global concentrations of CO2 and CH4 retrieved from GOSAT: first preliminary results. Sola 5, 160–163. https://doi.org/10.2151/sola.2009-041.

Zheng, B., Chevallier, F., Ciais, P., Broquet, G., Wang, Y., Lian, J., Zhao, Y., 2020. Observing carbon dioxide emissions over China's cities and industrial areas with the orbiting carbon Observatory-2. Atmos. Chem. Phys. 20, 8501–8510. https://doi.org/10.5194/acp-20-8501-2020.